NUMERICAL INVESTIGATION OF NATURAL CONVECTION IN POROUS MEDIA ENCLOSED BETWEEN TWO CONCENTRIC VERTICAL CYLINDERS

By

Atwan, E. F.*, El-Shazly, K. M.*, Khalil, E. E.** and Abdel-Salam, M.S.**

* Lecturers, Faculty of Engineering, Shoubra, Zagazig University
** Professors, Faculty of Engineering, Cairo University

ABSTRACT

In the present work, natural-convective heat transfer in square and tall annuli filled with saturated porous media was investigated numerically. Heat transfer and fluid flow results were obtained numerically for a wide range of the governing parameters. Those, and their respective ranges of values, considered here, are; $1 \le A \le 10$, $2 \le k \le 25$, and Darcy-Rayleigh number Ra^* up to 10000, where, A is the aspect (height-to-gap width) ratio and k is the radius ratio. The finite difference approximation was performed on the basic steady-state governing equations (mass, momentum and energy equations) and the Successive Overrelaxation point iterative technique (SOR) was used as the solution method. The temperature and velocity fields are presented. Results show that the average Nusselt number increases with increasing both Darcy-Rayleigh number and radius ratio, while decreases with increasing aspect ratio. Correlations for heat transfer rates in terms of the average Nusselt number, Nu_i, were obtained which give the inner cylinder average Nusselt number (based on the gap width, D) for the boundary layer regime ($Ra^* \ge 300$).

NOMENCLATURE

c_p	specific heat of fluid at constant pressure	(J/kg.K)
D	annulus gap width, $r_o - r_i$	(m)
g	gravitational acceleration	(m/s^2)
h	convective heat transfer coefficient	(W/m^2 K)
K	permeability of the porous medium	(m^2)
k	radius ratio, r_o/r_i	
k_e	thermal conductivity of saturated porous medium	(W/m.K)
L	height of the porous annulus	(m)
P	pressure	(N/m^2)
p(R)	transformed coordinate of R-direction	(m)
q(Z)	transformed coordinate of Z-direction	(m)
r	radial distance	(m)
T	temperature	(°C or K)

U_o	reference velocity	(m/s)
u	fluid velocity in radial direction	(m/s)
v	fluid velocity in vertical direction	(m/s)
z	cylindrical coordinate for vertical direction	(m)

Dimensionless Groups

A	aspect ratio, L/D
Nu_D	Local Nusselt number based on the gap-width, hD/k_m
Nu_i	Average Nusselt number based on the gap-width, hD/k_m
R	dimensionless radial distance, $(r-r_i)/D$
Ra^*	Darcy-Rayleigh number, $(g\beta K D\Delta T)/(\gamma\alpha)$
U	dimensionless velocity in r-direction, u/U_o
V	dimensionless velocity in z-direction, v/U_o
Z	dimensionless vertical distance, z/L

Greek Letters

α	thermal diffusivity of porous medium, $k_m/\rho c_p$	(m^2/s)
β	isobaric coefficient of thermal expansion	(K^{-1})
γ	relaxation factor	
ΔT	temperature difference	(°C or K)
μ	dynamic molecular viscosity	(kg/m.s)
η	radius ratio parameter, D/r_i	
θ	dimensionless temperature, $(T-T_o)/(T_i-T_o)$	
ν	kinematic viscosity of fluid	(m^2/s)
ρ	density	(kg/m^3)
Ψ^*	dimensionless stream function, $(D/\alpha r_i L)\Psi$	
Ψ	stream function	
ζ	dummy variable	

Subscripts

D	based upon annulus gap width
f	saturating fluid
i	inner wall (heated)
m	porous medium
o	outer wall (cooled)
r	reference point

Superscripts

—	average value
*	modified

1. INTRODUCTION

More recent motivation for study of natural convection in liquid-saturated annular porous media has come from efforts to identify a geologic repository for the storage of canisters containing high-level nuclear-waste materials. Geologic media

under investigation include deep-ocean seabed sediments and deep-earth rock layers, which are fully saturated with liquid water. Water motion throughout such media, induced by radioactive-decay/heat-release mechanisms, must be understood if one is to accurately predict canister/medium thermal response. The potential extent of radionuclide transport is also strongly dependent upon this thermally-induced velocity field. Canisters are expected to be long, slender cylinders, emplaced in the geologic medium parallel to the gravity vector. Constant lateral spacings between adjacent canisters, and between parallel rows of canisters, will be maintained based on total projected heat loads. Due to these considerations, the "single-canister" problem can then be reduced to the study of natural convection in a liquid-saturated porous medium bounded by vertical, coaxial cylinders.

In spite of the importance of convective heat transfer in vertical annular enclosures filled with saturated porous media in many practical applications, very few basic and comprehensive studies have so far been conducted for this system.

Reda [1] conducted experiments with constant heat flux on the inner wall for k=23, A=4.25, and $Ra^*<80$. Prasad and Kulacki [2] studied, numerically and experimentally, free-convective heat transfer in short cylindrical annuli filled with saturated porous media. The inner wall is heated at constant temperature and the outer wall is isothermally cooled, the top and bottom being insulated. Heat transfer results have been obtained numerically for $0.3 \le A \le 0.9$, $1 < k \le 11$ and Darcy-Rayleigh number, Ra^* up to 10^4. Their results indicate that the introduction of curvature effects diminishes the multicellular flow behaviour observed in the case of shallow cavity. They also conducted experiments for the porous media produced by water saturated glass beads of 3.0 mm and 6.0 mm diameters, for k=5.338, A=1, and $49 < Ra^* < 3582$. Hickox and Gartling [3] performed a numerical study of steady, natural convection in a fluid-saturated, vertical annular porous layer. Using a finite element technique and an approximate method, they have obtained heat transfer results for tall annulus ($A \ge 2$) and low Darcy-Rayleigh numbers, Ra^* up to 100. Havstad and Burns [4] investigated theoretically convective heat transfer in concentric vertical annulus filled with a porous medium. They used three different methods to investigate the problem: finite difference numerical method, perturbation technique, and an approximate analysis. Their work is applicable only for low Darcy-Rayleigh number. They have also presented a correlation for the heat transfer rates in terms of the average Nusselt number for $A \ge 1$, $0 < Ra^* < 150$ and $1 \le k \le 10$. Prasad, Kulacki, and Keyhani [5] conducted experiments on free convection in a

vertical annulus filled with a saturated porous medium for height-to-gap ratios of 1.46,1 and 0.545, and radius ratio of 5.338. In their experiments, the inner and outer walls were maintained at constant temperatures. Several fluid-solid combinations were used. David, Lauriet and Prasad [6] performed a numerical study on natural convection in a differentially heated vertical, annular porous layer to examine the appropriateness of a formulation based on the Darcy-Brinkman-Forchheimer equation of motion with variable porosity and stagnant thermal conductivity in the wall region. Prasad and Kulacki [7] studied, numerically, steady free convection in a vertical annulus filled with a saturated porous medium and of which the vertical walls are at constant temperatures, the horizontal walls being insulated. The numerical results obtained indicated that the curvature effects on temperature and velocity fields are significant, and completely disturb the centro-symmmetrical nature found in the vertical cavity case. Burns and Tien [8] carried-out an analytical investigation of natural convection in porous media completely enclosed by concentric spheres and horizontal cylinders. The steady, two-dimensional problem has been solved by the method of finite differences and the method of regular perturbations. The flow field has been examined and compared for the two geometries. More recent study for natural convection in a porous horizontal cylindrical annulus was carried out by Barbosa and Saatdjian [9].

The objectives of the present numerical study are to obtain heat transfer and fluid flow characteristics and temperature distributions for the isothermally heated vertical annuli for a wide range of the governing parameters A, k and Ra^* as well as the correlations between the average Nusselt number, Nu_i and governing parameters which mentioned above.

2. MATHEMATICAL FORMULATION AND NUMERICAL ANALYSIS

2-1 Modelling Assumptions

The physical model and the system of coordinates of the problem are illustrated schematically in Fig.(1). The vertical cylindrical annuli filled with saturated porous media. The inner wall is heated at constant temperature and the outer wall is isothermally cooled, the top and bottom walls being perfectly insulated. The following assumptions are considered as the porous medium is isotropic and homogeneous, local thermal equilibrium exists, two dimensional model will be considered, viscous heat dissipation in the energy equation is negligible, the fluid is assumed to be nonparticipating in any radiation, Boussinesq approximation is utilized, additional viscous drag

(Brinkman's model) and inertia terms are neglected, steady laminar axisymmetric conditions prevail, all walls of the annulus are further assumed to be impermeable and the dispersion effects are neglected in the present formulation.

2-2 Governing Equations

The governing equations expressing conservation of mass, momentum and energy where Darcy's law holds, and with the forgoing assumptions are:

continuity:

$$\frac{\partial}{\partial r}(ru) + \frac{\partial}{\partial z}(rv) = 0 \tag{1}$$

r-momentum:

$$u = -\frac{K}{\mu}\frac{\partial p}{\partial r} \tag{2}$$

z-momentum:

$$v = -\frac{K}{\mu}\left(\frac{\partial p}{\partial z} + \rho g\right) \tag{3}$$

energy:

$$u\frac{\partial T}{\partial r} + v\frac{\partial T}{\partial z} = \alpha\left[\frac{1}{r}\frac{\partial}{\partial r}\left(r\frac{\partial T}{\partial r}\right) + \frac{\partial^2 T}{\partial z^2}\right] \tag{4}$$

equation of state:

$$\rho = \rho_r\,[1-\beta(T-T_r)] \tag{5}$$

The equations above contain four unknowns namely the two velocity components, pressure, and temperature. Solving these expressions simultaneously, one can obtain their distribution over the flow field.

2.2.1 The boundary conditions:

Since all boundaries of the porous layer are impermeable, the velocity component normal to a boundary must vanish on the boundary, and hence;

$$u(r_i,z) = 0 = v(r_i,z) \tag{6a}$$
$$u(r_o,z) = 0 = v(r_o,z) \tag{6b}$$
$$u(r,0) = 0 = v(r,0) \tag{6c}$$
$$u(r,L) = 0 = v(r,L) \tag{6d}$$

Also, the horizontal boundaries are insulated; thus, the condition of zero heat flux normal to the boundary is imposed,

$$\frac{\partial T}{\partial z}(r,0) = 0 = \frac{\partial T}{\partial z}(r,L) \tag{6e}$$

The temperatures on the vertical boundaries, as indicated in Fig.(1), are specified by:

$$T(r_i,z) = T_i \tag{6f}$$

$$T(r_o,z) = T_o \tag{6g}$$

2.2.2 Stream function transformations:

For solving the forgoing governing equations (1) to (5), it is often preferred, however, to express these equations in the stream function form, which reduces the number of unknowns by one, eliminating the pressure variable. This is done by cross differen-tiating the two momentum equations and subtracting one from the other. On introducing the stream function (Ψ), the horizontal and vertical velocities are defined as:

$$u = -\frac{1}{r}\frac{\partial \Psi}{\partial z} \tag{7a}$$

$$v = \frac{1}{r}\frac{\partial \Psi}{\partial r} \tag{7b}$$

Using the above definitions of density variation and velocity components, the continuity equation is automatically satisfied and the energy equation and the momentum equation become:

Momentum:

$$\frac{\mu}{K}\left[\frac{\partial}{\partial r}\left(\frac{1}{r}\frac{\partial \Psi}{\partial r}\right) + \frac{\partial}{\partial z}\left(\frac{1}{r}\frac{\partial \Psi}{\partial z}\right)\right] = \rho_r g\beta \frac{\partial T}{\partial r} \tag{8}$$

Energy:

$$-\frac{1}{r}\frac{\partial \Psi}{\partial z}\frac{\partial T}{\partial r} + \frac{1}{r}\frac{\partial \Psi}{\partial r}\frac{\partial T}{\partial z} = \alpha\left[\frac{1}{r}\frac{\partial}{\partial r}\left(r\frac{\partial T}{\partial r}\right) + \frac{\partial^2 T}{\partial z^2}\right] \tag{9}$$

2.2.3 Non-dimensional governing equations:

Before undertaking a numerical solution, the first step should invariably be to place the equations to be solved in a dimensionless form as: Momentum equation:

$$0 = -\frac{\partial^2 \Psi^*}{\partial R^2} - \frac{1}{A^2}\frac{\partial^2 \Psi^*}{\partial Z^2} + \left(\frac{\Re}{1+\Re R}\right)\frac{\partial \Psi^*}{\partial R} + \frac{1}{A} - Ra^*\,(1+\Re R)\frac{\partial \theta}{\partial R} \tag{10}$$

Energy equation:

$$\frac{\partial \Psi^*}{\partial R}\frac{\partial \theta}{\partial Z} - \frac{\partial \Psi^*}{\partial Z}\frac{\partial \theta}{\partial R} = (\eta R+1)\frac{\partial^2 \theta}{\partial R^2} + \eta \frac{\partial \theta}{\partial R} + \frac{1}{A^2}(\eta R+1)\frac{\partial^2 \theta}{\partial Z^2} \qquad (11)$$

which may be expressed in a simpler form as :

$$U\frac{\partial \theta}{\partial R} + V\left(\frac{1}{A}\right)\frac{\partial \theta}{\partial Z} = \frac{\partial^2 \theta}{\partial R^2} + \frac{1}{A^2}\frac{\partial^2 \theta}{\partial Z^2} + \left(\frac{\eta}{1+\eta R}\right)\frac{\partial \theta}{\partial R} \qquad (12)$$

2.2.4 Non-dimensional boundary conditions

The forgoing boundary conditions eqs. (6a)-(6g) may be given in a dimensionless form as:

$$U(0,Z) = 0.0 = V(0,Z) \qquad (13a)$$
$$U(1,Z) = 0.0 = V(1,Z) \qquad (13b)$$
$$U(R,0) = 0.0 = V(R,0) \qquad (13c)$$
$$U(R,1) = 0.0 = V(R,1) \qquad (13d)$$
$$\frac{\partial \theta}{\partial Z}(R,0) = 0.0 = \frac{\partial \theta}{\partial Z}(R,1) \qquad (13e)$$
$$\theta(0,Z) = 1.0 \qquad (13f)$$
$$\theta(1,Z) = 0.0 \qquad (13g)$$
$$\Psi^*(0,Z) = 0.0 = \Psi^*(1,Z) \qquad (13h)$$
$$\Psi^*(R,0) = 0.0 = \Psi^*(R,1) \qquad (13i)$$

2.2.5 Local and average Nusselt numbers:

The local Nusselt number is calculated as :

$$Nu_D = -A\frac{D}{L}\frac{\partial \theta}{\partial R}\bigg|_w = -\frac{\partial \theta}{\partial R}\bigg|_w \qquad (14)$$

and, the average Nusselt number on the inner wall based on the gap width is given by:

$$\overline{Nu_i} = -\int_0^1 \frac{\partial \theta}{\partial R}\bigg|_{R=0} dZ \qquad (15)$$

The average Nusselt numbers on the inner and outer walls are related by:

$$\overline{Nu_o} = \left(\frac{1}{k}\right)\overline{Nu_i} \qquad (16)$$

In light of equation (16), there is no need to give

separate consideration to Nu_i and Nu_e, and attention will subsequently be focused on Nu_i. We thus anticipate the following functional relationship among the various non-dimensional parameters;

$$\overline{Nu_i} = f(Ra^*, A, k) \quad (17)$$

It is the functional relationship which is to be investigated numerically.

2.3 Numerical Procedure

For a numerical solution procedure of the momentum and energy equations (10) and (12), they are usually directly transformed into finite difference equations with the aid of a proper differencing scheme. But to account for the boundary layers near the side walls, one would have to introduce an extremely dense grid. This situation can be improved by introducing suitable transformation equations, p(R) and q(Z) proposed by Kùblbeck [10], which accumulate the grid points in the boundary layer region.

The conservation equations are transformed into difference equations by using a finite-difference scheme because the boundary conditions are unambiguous and smooth and the finite difference method is known to be successful on very similar problems [11], specially natural convection in enclosures and natural convection in porous media filled enclosures [8]. The finite difference representations are performed for all terms of the comprehensive form of momentum and energy equation, where The first and second derivatives of the diffusion and buoyancy terms are approximated by centered finite-difference scheme which has second-order accuracy with regard to truncation errors.

The Successive Overrelaxation iterative technique (SOR) is chosen as the method of solution. This is a relatively simple point iterative method which is based on the immediate use of the new updated values wherever possible and results in the dimensionless temperature in the case of solving the energy equation,and the dimensionless stream function in the case of solving the momentum equation. This method slows down the convergence but it is useful where steep gradients are present. In the present study the underrelaxation factor (γ) varied from 0.2 to 1.0, while the overrelaxation factor always taken 1.0.

2.3.1 Computational approach:

With using SOR scheme, θ and ψ^* are given initial approximate values at all interior grid points and the scheme solves for

θ and Ψ^* successively marching from left to right and from bottom to top and making use of the new values as soon as they are available. This procedure is repeated until the change between the new and old values of the temperature or stream function normalized with the old value is smaller than a prescribed tolerance at each point in the domain. Because of the symmetry, computations were carried out for only the right half of the annulus (Fig. 1). This region will be referred to as the "half-annulus". Upon completion of solution for a particular aspect ratio A, radius ratio k,and Darcy-Rayleigh number Ra^*, the Ra^* is continually increased until convergence is no longer obtainable. One full iteration cycle takes approximately 2 sec. The number of iterations required for convergence varies greatly ranging from 110 to about 550, being dependent on the aspect ratio A, the Darcy-Rayleigh number Ra^* , the radius ratio k, and the relaxation factor γ. The computations were performed on a digital 486 microcomputer using a FORTRAN program .

2.3.2. NUMERICAL STABILITY AND CONVERGENCE

To judge the iterative convergence of the solution for the present computations, the following criterion was used

$$\left| \frac{\zeta^{n+1} - \zeta^{n}}{\zeta^{n}} \right| \leq 5 \times 10^{-3} \qquad (18)$$

at each point in the domain for both the temperature, θ, and the stream function, Ψ^*. The superscripts n and n+1 indicate the values at a given node on two successive iterations.

In order to properly select the mesh size, various combinations of mesh sizes were used to select one which gives better accuracy and requires less computational time. It was observed that the use of varying grids with fine mesh near the walls is advantageous and more reasonable for high Darcy-Rayleigh numbers owing to boundary layers on the vertical walls and significant changes in the magnitude and direction of the velocities near the horizontal walls. Computations were carried out with 9x9 to 63x63 non-uniform grids, for aspect ratio A=5.0 and the CPU time was recorded.

Figure (2) shows the effect of mesh size on the inner cylinder average Nusselt number and CPU time for A=5.0, k=4.16, and Ra^*=2000. For the present problem, a 31x31 non-uniform grid was selected which yields Nusselt numbers within 2 percent of the values obtained by using very fine grid sizes (63x63).

An additional test of the accuracy of the numerical procedure employed in the present study is presented in Fig.(3). It was observed that the present results agree well with numerical solutions of Prasad and Kulacki [7] though their results are a little lower for $Ra^*>1000$.

The agreement between the results obtained from the approximate analysis by Hickox and Gartling [3] and the present results is also quite good for low Darcy-Rayleigh numbers up to $Ra^*=200$ which covers the range through which the assumptions made in their analysis, was valid.

3. Results and Discussion

3.1. ANALYSIS OF THERMAL AND FLOW FIELDS RESULTS

Numerical results are obtained for a wide range of the governing parameters, Darcy-Rayleigh number (based on the gap width) up to 10000, radius ratio ranged from 2 to 25 and aspect ratio (annulus height/gap width) ranged from 1 to 10.

Figure (4) depicts streamlines and isotherms predicted with the aid of the numerical scheme for an annulus of A=1, radius ratio k=8, and Darcy-Rayleigh numbers $Ra^*=10$, 100 and 5000. Inspection of these maps shows that, as the Darcy-Rayleigh number increases a circulatory motion is established due to buoyancy effects. The flow consists of a single cell filling the entire half-annulus and rotating slowly in the clockwise direction (counter clockwise in the other half). The upper inside and lower outside regions are relatively stagnant. As Ra^* is increased further, the streamlines move closer to the cold wall, producing strong boundary layer effects on the side wall.

This behaviour of the streamlines is explained as the fluid rises along the inner vertical hot wall and warms up, a higher pressure region develops in the upper inside corner. The flow must turns towards the outside away from the corner, leaving a large fairly stagnant region. As the flow approaches the outside wall it cools and descends abruptly. Another high pressure stagnant zone develops in the lower outside region and the flow turns towards the inside as it falls. In the lower inside region, the fluid warms and abruptly begins to rise. The same behaviour is obtained with increasing radius ratio and decresing aspect ratio. More isotherms and streamlines maps can be referred to Atwan thesis [12]. It may be noted that this general behaviour of the core-region flow is qualitatively very similar to free convective flows for Newtonian fluids [13, 14] though no multi-cellular flow is observed in the present case.

Figures (5a-f) present the numerical predictions of the typical

non-dimensional temperature, θ with the non-dimensional radial distance, R at various heights, z/L=0.00, 0.25, 0.50, and 0.75 for some selected values of Darcy-Rayleigh number Ra^*, aspect ratio A, and radius ratio k. An increase in the Darcy-Rayleigh number results in a stably stratified temperature distribution and the extent of this stratified temperature distribution continually increases with increasing the Darcy-Rayleigh number Ra^* producing a thermal boundary layer on the vertical walls (high temperature gradients), indicating strong natural convection flow as shown in Fig.(5a&b). The sink temperature for the boundary layer on the hot wall reduces as the radius ratio increases and this enhances the heat transfer rate in terms of the average Nusselt number. Also, for high radius ratios, the conduction in the core is very small for any given Ra^* and A as shown in Figs.(5c&d). As the aspect ratio increases the decrease in temperature near the hot wall becomes less, and hence, the temperature gradients near the hot wall decrease, indicating less natural convection flow as shown in Figs.(5e&f). These results are consistent with the predicted streamlines and isotherms explained before.

3.2. ANALYSIS OF HEAT TRANSFER RESULTS

3.2.1. Local Nusselt numbers

The predicted local Nusselt numbers on the inner and outer vertical, Nu_D, are presented in Fig.(6) for some selected values of Darcy-Rayleigh number Ra^*, aspect ratio A, and radius ratio k. It can be seen that the maximum in the local Nusselt number on the inner heated wall, Nu_{Di}, occures at the lower edge (Z=0.0) and then drops as Z increases and reaches its lower value near the top wall (Z=1) as shown in Fig.(6a). This behaviour is consistent with the thermal and flow fields presented before. The higher the radius ratio or the lower the aspect ratio, the higher the heat transfer rate in terms of the average Nusselt number and this clearly indicated by the area under the curve of Nu_{Di} versus Z.

On the cold wall, the case is reversed. The rate of heat transfer is very high near the top edge as clearly shown in Fig.(6b), indicating that a large percentage of heat being rejected in a very small distance from the top. For higher aspect ratios and/or higher radius ratios, the heat transfer is further enhanced near the top edge.

3.2.2. Average Nusselt Numbers

The predicted heat transfer rates in terms of the average Nusselt number on the inner heated wall are presented in Figs.(7) and (8). The rate of increase of the

average Nusselt number decreases as the radius ratio increases when the Darcy- Rayleigh number is high as clearly shown in Figure (7) , where, for Ra^*= 10000 and A=10, the slope of the curve at k=25 is seen to be very small (Fig.7). This is not true for low Darcy-Rayleigh numbers. Actually,for pure conduction, the slope of $\ln(Nu_i)$ versus $\ln(k)$ curve increases with an increase in k (the conduction line). The overall conclusion is that the slope of the curve for $\ln(Nu_i)$ versus $\ln(k)$ is not a constant with respect to the radius ratio, where, the variation in the slope is high for low radius ratios and is small for high values of k. Also, If the radius ratio k is increased too much, the higher the Darcy-Rayleigh number required to establish the convective flows (boundary layer flow).

An increase in aspect ratio decreases the average Nusselt number as shown in figure (8). As the Darcy-Rayleigh number decreases, the rate of decrease becomes less.

3.3. NUSSELT NUMBER CORRELATIONS

The average Nusselt numbers may be correlated according to the relation:

$$Nu_i = a\, Ra^{*b}\, A^c\, k^d \qquad (19)$$

The values of the coefficients a, b, c and d are obtained from a least squares fit of the numerical results. The correlations obtained are:

For an annulus of A=1 (square annulus)

$$\overline{Nu_i} = 0.49626\, Ra^{*\,0.5184366}\, k^{0.2190643} \qquad (20)$$

$$300 \le Ra^* \le 10000$$
$$2 \le k \le 25$$

For an annulus of A≥3 (tall annulus)

$$\overline{Nu_i} = 0.5835058\, Ra^{*\,0.4931295}\, A^{-0.4645421}\, k^{0.2886357} \qquad (21)$$

$$300 \le Ra^* \le 10000$$
$$2 \le k \le 25$$
$$3 \le A \le 10$$

The predicted values are within 12 percent of the computed ones for the square and tall annuli. A further subdivision of the data would not have results in a significant improvement in the mean deviation of the correlations. The above deviations between the predicted and the computed numerical values are mainly due to the

continuous change in the slope of the $\ln(Nu_i)$ vs $\ln(k)$ curves, and the lower slope of the curve for high Darcy-Rayleigh numbers and large radius ratios.

3.4. COMPARISON WITH PREVIOUSLY PUBLISHED RESULTS

A graphical comparison of the present correlations based on the numerical results with those of Hickox and Gartling [3], Havstad and Burns [4], and Prasad and Kulacki [7] is presented in Fig.(9). The present results are from 6.5 percent to 13.6 percent higher than those reported by them. In general, the comparison of results is considered satisfactory.

4. CONCLUSIONS

The temperature and velocity fields, and consequently the heat transfer rates in terms of the average Nusselt number, are not only functions of Darcy-Rayleigh number Ra^* and aspect ratio A, but depend strongly on the radius ratio k.

An increase in the radius ratio and/or Darcy-Rayleigh number enhances the heat transfer coefficient in terms of the average Nusselt number by modifying the temperature field such that the effective sink temperature for the boundary layer on the inner wall decreases and becomes much closer to the outer wall temperature.

An increase of aspect ratio results in less stratification of temperature distribution in the core region which indicates less temperature gradients near the hot wall, and hence, less convective heat transfer rates in terms of the average Nusselt numbers.

A large percentage of heat is being rejected in a very small distance from the top edge of the cold wall. The higher the aspect ratios and/or lower the radius ratios, the higher is the heat transfer rate in the top portion.

The heat transfer rates in terms of the inner cylinder average Nusselt number are correlated separately for the numerical results.

REFERENCES

1. Reda, D.C., "Natural Convection Experiments in a Liquid-Saturated Porous Medium Bounded by Vertical Coaxial Cylinders," Trans. ASME, Journal of Heat Transfer, vol. 105, pp. 795-802, Nov. 1983.
2. Prasad, V. and Kulacki F.A., "Natural Convection in Porous Media Bounded by Short Concentric Vertical Cylinders," Trans. ASME, Journal of Heat Transfer, vol. 107, pp. 147-154, Feb. 1985.
3. Hickox, C.E. and Gartling, D.K.,"A Numerical Study of Natural

Convection in a Vertical, Annular, Porous Layer," ASME, Paper No. 82-HT-68, 1982.
4. Havstad, M.A. and Burns, P.J., "Convective Heat Transfer in Vertical Cylindrical Annuli Filled With A Porous Medium," Int. J. Heat Mass transfer, vol. 25, No. 11, pp. 1755-1766, 1982.
5. Prasad, V., Kulacki, F.A. and Keyhani, M., "Natural Convection in Porous Media," Journal of Fluid Mechanics, vol. 150, pp.89-119, 1985.
6. David, E., Lauriat, G. and Prasad, V., "Non-Darcy Natural Convection in Packed-sphere Beds Between Concentric Vertical Cylinders," AIchE Symposium Series, vol. 85 n. 269, pp. 90-95, 1989.
7. Prasad, V. and Kulacki, F.A., "Natural Convection in a Vertical Porous Annulus," Int. J. Heat Mass Transfer, vol. 27, No. 2, pp. 207-219, 1984.
8. Burns, P.J. and Tien, C.L., "Natural Convection in Porous Media Bounded by Concentric Spheres and Horizontal Cylinders," Int. J. Heat Mass Transfer, vol. 22, pp. 929-939, 1978.
9. Barbosa Mota, J. P. and Saatdjian, E. "Natural Convection in a Porous, Horizontal Cylindrical Annulus", J.of Heat Transfer, ASME, Vol. 116, pp 621-626, 1994
10. Kublbeck, K., Merker, G.P. and Straub, J., "Advanced Numerical Computation of Two-Dimensional Time-Dependent Free Convection in Cavities," Int.J. Heat Mass Transfer, vol. 23, pp. 203-217, 1980.
11. Hornbeck, R.W., "Numerical Marching Techniques for Fluid Flows with Heat Transfer," Scientfic and Technical Information Office, National Aeronautics and Space Administration, Washington, D.C., 1973.
12. Atwan, E. F., " Numerical and Experimental Investigation of Natural Convection in Porous Media Enclosed Between Two Concentric Vertical Cylinders", Ph. D. Thesis, Cairo University, 1994.
13. De Vahl Davis, G. and Thomas, R.W., "Natural Convection Between Concentric Vertical Cylinders," High Speed Computing in Fluid Dynmics, Physics of Fluids, Supplement II, pp. 198-207, 1969.
14. Thomas, R.W. and De Vahl Davis, G., "Natural Convection in Annular and Rectangular Cavities- A Numerical Study," Proceedings, Fourth International Heat Transfer Conference, Paris, vol. 4, Paper NC 2.4, Elsevier, Amsterdam, 1970.

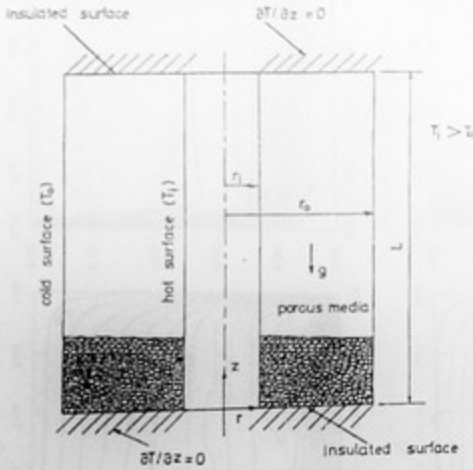

Fig. (1): Physical model of the vertical annulus, coordinate system and thermal boundary conditions.

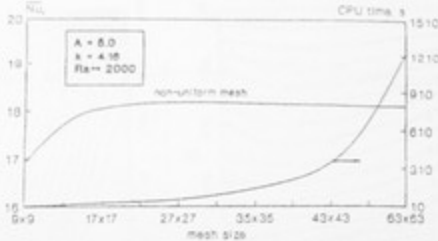

Fig. (2): Effect of mesh size on average Nusselt number and CPU time for A=6, k=4.16, and $Ra^*=2000$

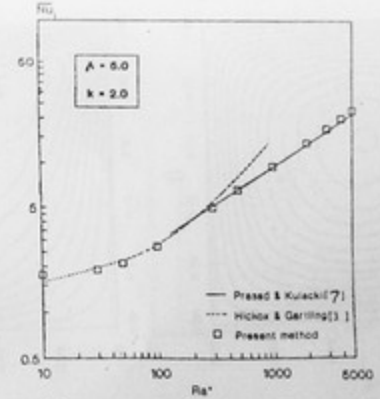

Fig. (3): Numerical accuracy test: Comparison between the present results and those previously published

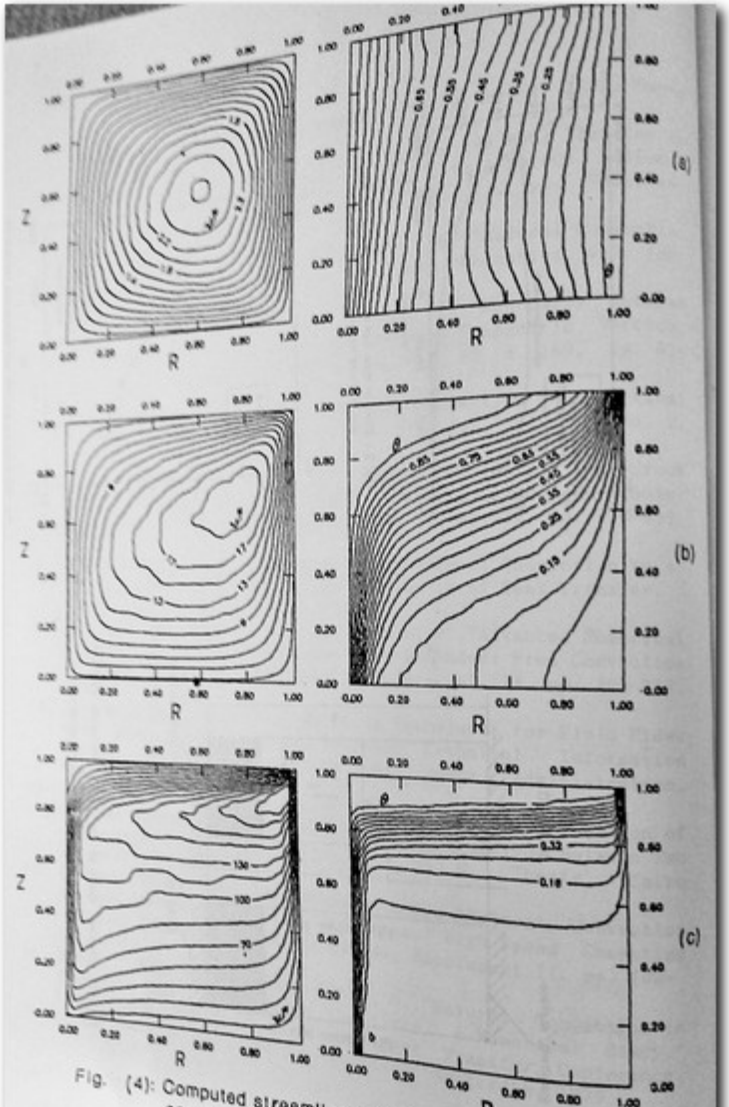

Fig. (4): Computed streamlines and isotherms for a vertical square annulus, A=1, k=8 for:
a) $Ra^*=10$ b) $Ra^*=100$ c) $Ra^*=5000$

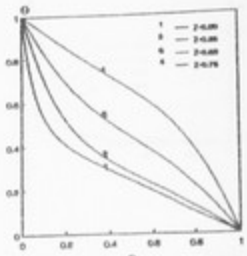

Fig.(5a): Temperature distribution for A=1.0, k=2 and Ra^=50

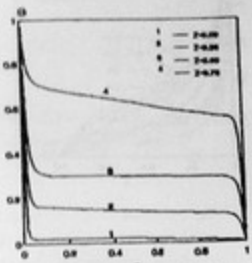

Fig.(5b): Temperature distribution for A=1.0, k=2 and Ra^=10000

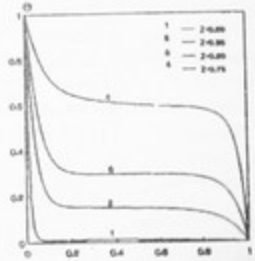

Fig.(5c): Temperature distribution for A=5.0, Ra^=8000 and k=2

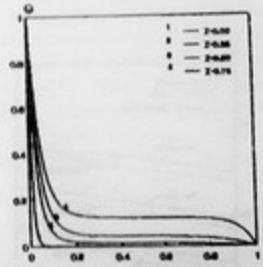

Fig.(5d): Temperature distribution for A=5.0, Ra^=8000 and k=80

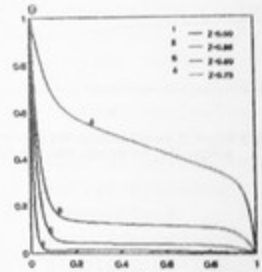

Fig.(5e): Temperature distribution for k=5, Ra^=9000 and A=1

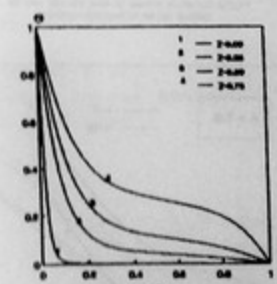

Fig.(5f): Temperature distribution for k=5, Ra^=9000 and A=10

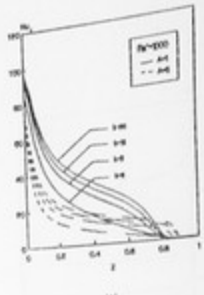

(a)

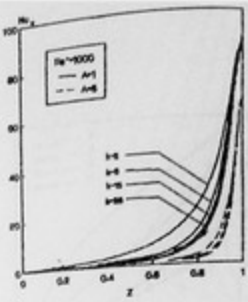

(b)

Fig(6): Variation of local Nusselt number, Nu on vertical walls for Ra*=1000
a) On inner heated wall b) On outer cold wall

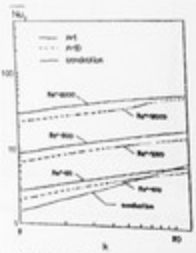

Fig(7) Curves effects on heat transfer rate for various values of Rayleigh numbers

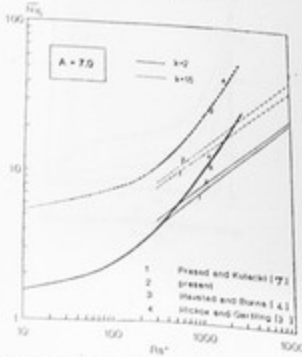

Fig(9): Comparison between the present and earlier published correlations

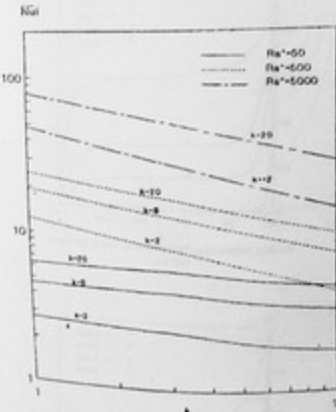

Fig(8): Effect of aspect ratio on the average Nusselt number, $\overline{Nu}_L$, for Ra*=50, 600, and 5000